2006

The Radiative Transport of Dust in Primordial Galaxies and Second-Generation Star Formation

Aparna Venkatesan
University of San Francisco, avenkatesan@usfca.edu

Biman B. Nath

J Shull

Recommended Citation
Aparna Venkatesan, Biman B. Nath, and J. Michael Shull. The Radiative Transport of Dust in Primordial Galaxies and Second-Generation Star Formation. The Astrophysical Journal, 640:31-40, 2006 March 20. DOI: 10.1086/500078

The Astrophysical Journal, 640:31–40, 2006 March 20

THE RADIATIVE TRANSPORT OF DUST IN PRIMORDIAL GALAXIES AND SECOND-GENERATION STAR FORMATION

Aparna Venkatesan,[1] Biman B. Nath,[2,3] and J. Michael Shull
CASA, Department of Astrophysical and Planetary Sciences, University of Colorado, Boulder, CO 80309-0389;
aparna@casa.colorado.edu, biman@rri.res.in, mshull@casa.colorado.edu
Received 2005 August 5; accepted 2005 November 27

ABSTRACT

We investigate the radiative transport of dust in primordial galaxies in the presence of the UV radiation field from the first metal-free stars. We find that dust created in the first supernova (SN) explosions can be driven through the interior of the SN remnant to accumulate in the SN shells, where second-generation stars may form from compressed cooling gas. This scenario requires metal-free stars to form continuously over timescales of up to 10 Myr, consistent with recent estimates. Silicate and graphite grains, as well as iron-bearing magnetites, are transported to the shells for reasonable parameter assumptions, but their relative yields from primordial SNe is an important factor in the resulting abundance ratios. We compare the results of segregated grain transport with the current nucleosynthetic data on extremely metal-poor Galactic halo stars. Fossil signatures of this process may already have been detected in those iron-poor stars with enhanced carbon and silicate elements such as magnesium, silicon and oxygen. We discuss the implications of our results for the transition from first- to second-generation star formation in primordial galaxies, and the role played by the radiative transport of dust in this process.

Subject headings: cosmology: theory — dust, extinction — galaxies: high-redshift — stars: abundances — stars: Population II — supernova remnants

1. INTRODUCTION

The radiative transport of dust and the grain history in galaxies have been studied by many authors, generally in the context of our Galaxy (e.g., Draine & Salpeter 1979a; Dwek & Scalo 1980; Seab & Shull 1983). Although early calculations (Pecker 1972) of this problem indicated that dust transport was difficult to accomplish, Ferrara et al. (1991) found that it was possible to transport dust grains by radiation pressure to large distances from the plane of the disk in a relatively short time ($\sim 10^8$ yr). In addition, dust destruction mechanisms are important to consider (Shustov & Vibe 1995).

In general, smaller dust grains are destroyed at a faster rate while they are being transported, and they typically do not survive. Grain destruction in the interstellar medium (ISM) occurs through thermal sputtering in hot gas, as well as nonthermal processes (sputtering, shattering, and vaporization in grain-grain collisions). The nonthermal processes occur primarily when the grains are swept up by shock waves (Shull 1978; Jones et al. 1994). In these situations, the original power-law grain size distribution will be modified by various processes of grain destruction (Seab & Shull 1983; Jones et al. 1996). Grains can also be accelerated through the gas by radiation fields. However, at a given radiation pressure, it is more difficult to drive large grains because of their lower ratio of area to mass. The final outcome of the radiative transport of dust therefore depends on the size and composition of the grains, as well as the details of the radiation field.

More recently, numerical simulations in a cosmological context have studied the radiative ejection of dust grains to the intergalactic medium (IGM) from primordial halos in the wake of the first generations of supernovae (SNe; Aguirre et al. 2001; Bianchi & Ferrara 2005). Testing the predictions of such theories of cosmological dust transport has usually been done in a macroscopic context, using upper limits from the cosmic microwave background to constrain IGM dust distortion (Loeb & Haiman 1997; Ferrara et al. 1999) or to offer alternative explanations to a cosmological constant scenario of the data on Type Ia SNe at redshifts $z \lesssim 2$ (Aguirre 1999).

In this paper, we focus on more local effects of dust transport within the host galaxy related to second-generation stars that form coevally with or subsequent to primordial stars. We examine, under the conditions in typical primordial halos, whether dust can be driven effectively by the radiative pressure of metal-free stars. If so, can dust grains accumulate in the cooling shells of first-generation SN remnants (SNRs), becoming incorporated eventually into new star-forming sites? Recent work by Mackey et al. (2003) and Salvaterra et al. (2004) suggest that such second-generation star formation is highly likely, forming from metal-poor or even metal-free fragmenting gas in SN shells in early galaxies. The latter authors show that instabilities in the SN shell that could lead to gas fragmentation and to the eventual formation of low-mass second-generation stars set in at about 1–50 Myr after the SN explosion. This range holds for the condition that the SN shells do not sweep the baryons out of a galaxy of virial temperature 10^4 K. A timescale requirement of $\sim$a few Myr to 10^8 yr is entirely consistent with the duration of metal-free star formation calculated by both semianalytic (Tumlinson et al. 2004) and numerical methods (Wada & Venkatesan 2003; Bromm et al. 2003). These involve estimates of the timescales over which metals from the first SNe can enrich the gas in either the host galaxy or neighboring galaxies. We motivate this hypothesis by considering the currently available element abundance ratios of extremely metal-poor (EMP) stars in the Galactic halo. The elements composing the dominant dust compounds from the first SNe, including C, Si, O, and Fe, in addition provide the most effective cooling channels for primordial star-forming gas (Bromm & Loeb 2003; Santoro & Shull 2006).

[1] NSF Astronomy and Astrophysics Postdoctoral Fellow.
[2] JILA Visiting Fellow, University of Colorado and National Institute of Standards and Technology.
[3] Raman Research Institute, Bangalore, 560-080, India.

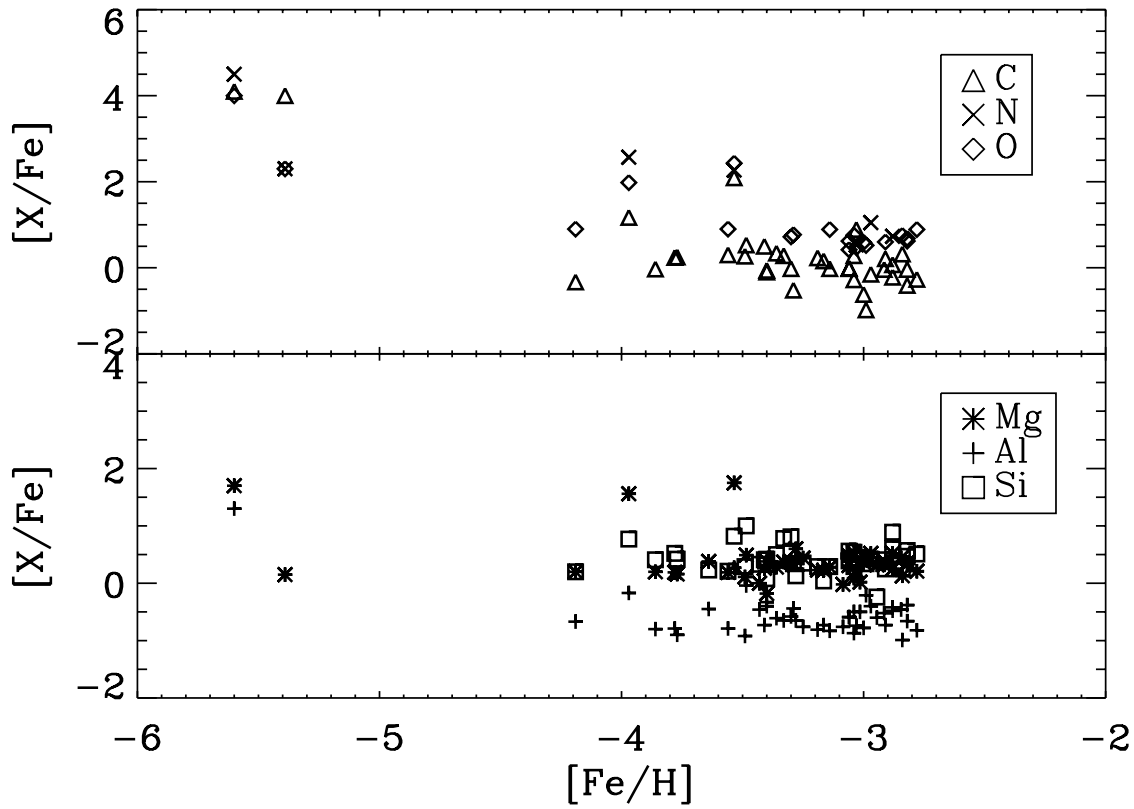

FIG. 1.—Observed abundances of (*top*) C, N, O, and (*bottom*) Mg, Al, and Si relative to Fe as a function of [Fe/H] in EMP halo stars. See text for discussion.

The paper is organized as follows. In § 2, we present the current nucleosynthetic data on EMP stars to motivate the consideration of a dust transport scenario. In § 3, we describe the formalism and assumptions of the model used to solve for dust grain transport, the results of which are presented in § 4. We discuss implications of our findings and conclude in § 5.

2. NUCLEOSYNTHETIC DATA ON EMP STARS

We begin by using the current data on EMP stars relevant for the problem in this paper. We highlight the trends of carbon, silicon, oxygen, nitrogen, magnesium, and aluminium as a function of iron abundance below [Fe/H] ~ -2.8. These elements, with the exception of nitrogen, are the most relevant for dust creation from the metals from the SNe of metal-free stars (Schneider et al. 2004; Todini & Ferrara 2001). We define [Fe/H] as the ratio of the measured column densities of Fe/H to the solar ratio, $(\mathrm{Fe/H})_{\odot} = 4.68 \times 10^{-5}$.

The nature of the primordial stellar initial mass function (IMF) is currently of great interest and debate. Some recent theoretical studies indicate that this IMF may have been top-heavy (Abel et al. 2000; Bromm et al. 2002), leading predominantly to stellar masses $\gtrsim 100\ M_{\odot}$ up to a critical gas metallicity of $Z_{\mathrm{cr}} \approx 10^{-4\pm1}\ Z_{\odot}$ (Bromm et al. 2001a; Schneider et al. 2002), above which a present-day IMF occurs. However, other detailed studies of the current data on reionization, high-z star formation, and the metal abundance ratios in the IGM and EMP stars suggest that the primordial IMF, rather than being biased toward high masses, may merely lack low-mass stars (Venkatesan & Truran 2003; Tumlinson et al. 2004; Daigne et al. 2004; Qian & Wasserburg 2005). It is certainly possible that both IMFs were coeval in the past, given the right combination of conditions, as pointed out in these papers. In addition, the transition metallicity Z_{cr} may be significantly higher at low densities and could vary with metal species (Bromm & Loeb 2003; Santoro & Shull 2006). These two IMFs, $\gtrsim$100 and $\sim$10–100 $M_{\odot}$, represent two possibilities in the definition of a top-heavy IMF, where the IMF's lower or upper mass limit is increased. A third option would be to flatten the slope or alter the shape of the stellar IMF.

Regardless of such IMF issues, we expect the first generations of stars to form from metal-free gas. Their composition heavily influences their structure and properties, as they rely predominantly on the p–p chain initially than on the more efficient CNO cycle for their thermonuclear fuel source (Tumlinson & Shull 2000). Consequently, metal-free stars are hotter and emit significantly harder ionizing radiation relative to their finite-Z counterparts (Bromm et al. 2001b; Tumlinson et al. 2003; Schaerer 2002). This will play an important role for the dust transport problem here.

Stars of masses $\sim$10–100 $M_{\odot}$ end their lives as the more familiar Type II SNe, leaving behind neutron stars and black holes, whereas metal-free stars in the mass range $\sim$140–260 $M_{\odot}$ are thought to disrupt themselves entirely as pair-instability SNe (PISNe). We do not concern ourselves here with the exact type of SN in primordial halos and require only that the parent metal-free stellar cluster have effective luminosities of $\sim 10^6\ L_{\odot}$ (Tumlinson et al. 2003; Bromm et al. 2001b; Schaerer 2002), which is easily achieved by a few tens of stars in a Salpeter IMF in the 1–100 $M_{\odot}$ range or a single star of mass $\gtrsim 100\ M_{\odot}$. For the purposes of this paper, we require the former case, i.e., a stellar cluster, so that there is a hard photon source for at least a few to 10 Myr after the initial SN explosion. We also require that the SN kinetic energy be at least 10^{51} ergs, which is true for "normal" Type II SNe. We discuss the case of hypernovae (HNe) below; the SN explosion energies for HNe and PISNe are thought to lie in the range 10^{51}–10^{53} ergs (Umeda & Nomoto 2003; Heger & Woosley 2002).

In Figure 1, we show the measured EMP stellar abundances of C, N, O, Mg, Al, and Si relative to Fe (normalized to the solar ratio), as a function of [Fe/H]. We limit the data to those EMP

stars with $[Fe/H] \lesssim -2.8$, to be consistent with the upper limit to the transition metallicity, factoring in typical errors in the data of order 0.1–0.2 dex. This is also close to the upper limit in metallicity derived by Salvaterra et al. (2004) for second-generation stars forming in the SN-induced scenario. We take the data of EMP giants from the study by Cayrel et al. (2004) and of EMP dwarfs and other stars from Cohen et al. (2004), Aoki et al. (2004), Tumlinson et al. (2004), and references therein. For the two most iron-poor stars, HE 0107−5240 and the newly discovered HE 1327−2326, we use the published abundances by Christlieb et al. (2004) and Frebel et al. (2005).

We note some relevant points of interest in Figure 1. First, although the two most iron-poor stars have greatly enhanced values of C, N, and O, there is no overall clear trend of [C/Fe] with [Fe/H]. We also observe that those EMP stars with highly enhanced C (the so-called C-enhanced EMPs)[4] also have strong N overabundances relative to solar, sometimes even exceeding that of C. Oxygen, on the other hand, is usually enhanced, sometimes up to 10^2–10^4 times solar at the lowest Fe-metallicities. We note also the consistent enhancements of Mg and Si of a few to 100 times solar and the relatively flat mild underabundance of [Al/Fe] with [Fe/H].

Several models have been proposed to explain the diversity of element abundances in low-mass EMP stars. Some interpret the abundances as reflecting the star's gas formation conditions, while others invoke processes subsequent to its creation. The presence of Mg and heavier elements would argue for the former class of models in principle. Among these, the HN model (Umeda & Nomoto 2003) is currently the most successful at reproducing the EMP data, requiring a new class of SN at primordial metallicities that have enhanced SN explosion energies of 10^{51}–10^{53} ergs and enhanced CNO element generation relative to Fe at low [Fe/H]. HN models can reproduce most EMP element abundances well, except N and Na, but they require significant fine-tuning for each EMP star, with the appropriate ratio of mixing, fallback, asymmetry, and/or jets in the SN model. The postformation scenarios include the dredge-up of elements during the star's giant branch phase, accretion from the interstellar medium or a companion star, and the rotation of the parent star—all of these could enhance C, N, O, and sometimes Mg given enough time. The joint trend of enhanced Mg, Si, and O at low [Fe/H], however, remains unexplained. The strong variations between individual EMPs among the elements shown here and those related to the Fe-peak and *r*- and *s*-process elements imply that any successful scenario may require considerable tailoring for each star.

Although N is not an element of much relevance to dust, we include it here, as it is usually a good tracer of C and O, because of its origin in the CNO cycle and hence of the asymptotic giant branch (AGB) scenario. We note that we have excluded stars known or thought to be in binaries, so we do not necessarily expect to see the signature of AGBs in binaries in Figure 1. Unfortunately, the data on N in this range of [Fe/H] are fairly scant, and no firm trend can be stated. As noted by Plez & Cohen (2005), EMP stars with enhanced C usually have enhanced N as well, but the reverse is not always true. This is seen in Figure 1. It is possible that N depletion can occur through the formation of ammonia (NH_3) ices as mantles on grains in dense clouds, but these likely are sputtered away immediately.

[4] Selecting merely on the basis of C-enhancement is unlikely to narrow down the parent process, as many C-enhanced EMP stars show selective enhancements of *r*- and *s*-processes, as well as other elements. As many authors have discussed, this great diversity of abundance ratios may indicate an equal diversity of contributing mechanisms.

In contrast, although not shown here, it is worth noting that for the few stars with measured CNO abundances that have $[Fe/H] \gtrsim -3$, [C/Fe] is mildly underabundant, whereas [N/Fe] is mildly overabundant, an anticorrelation noted by Briley et al. (2004) in a study of Galactic globular clusters. The varied behavior of N/C and the lack of a trend with [Fe/H] in EMP stars is noted in Plez & Cohen (2005), who point out that the SN origin is attractive because of the additional enhancement of Na, Mg, and especially O in these stars. The increasing enhancement of N accompanied by a decline of C as the star's evolutionary state advances would argue for self-enrichment from dredge-ups and other processes in the giant branch phase, but this is not observed.

In summary, the data on EMP stars indicate that Si, Mg, and O, and, to a lesser degree, C, are generally enhanced in the iron-poor stars. These elements form the composition of the dominant dust compounds created in SNe from metal-free stars of masses $\sim$10–260 $M_\odot$ (Todini & Ferrara 2001; Nozawa et al. 2003; Schneider et al. 2004), which include graphites, silicates (enstatites [$MgSiO_3$], forsterites [Mg_2SiO_4], and SiO_2), and iron-bearing magnetites. We therefore proceed to investigate whether these elements can be selectively transported in a hot radiation field, decoupled from the background SN metals in the gas phase.

3. CREATION AND TRANSPORT OF DUST GRAINS

In this section, we describe the scenario in which dust is created in primordial SNe, followed by a summary of the assumptions and equations we use to solve for the transport of dust grains.

3.1. *Dust Formation*

As discussed earlier, the duration of metal-free star formation is thought to be $\sim$10–100 Myr. The lower limit of a few–10 Myr has been derived using semianalytic calculations of halo self-enrichment from SN ejecta (Tumlinson et al. 2004) and from three-dimensional gas hydrodynamic simulations of the chemodynamical feedback from the first SNe on parsec scales in the ISM of primordial galaxies (Wada & Venkatesan 2003). In both analyses, this corresponds to the intrahalo timescale for the reincorporation of metals created by the first SNe into cold star-forming gas clumps up to metallicities roughly corresponding to Z_{cr} in primordial galaxies. The upper limit of 100 Myr corresponds to the interhalo enrichment timescale over which metals are transported to and pollute neighboring halos at $z \sim 10$–20 (Tumlinson et al. 2004; Bromm et al. 2003).

Such estimates are consistent with the 1–50 Myr timescales needed for the instability in SN shells to set in for second-generation star formation (Salvaterra et al. 2004). Stated another way, this timescale is a requirement for the model in this work, where the dust generated in the very first SNe, presumably on timescales of order 2–5 Myr, is exposed to the hot radiation field from a zero-metallicity stellar cluster that is assumed to be within the SNR. We focus on the effects of an individual SN in a stellar cluster and assume for simplicity that it occurs at the center of its host galaxy. A Population III cluster is likely to form with only a few stars in the densest part of the galaxy, and the massive stars in the Population III IMF likely have not migrated too far from their birthsites at $z \gg 10$. The specific location may not matter much for this work, as we are interested in relatively local rather than intergalactic transport.

A related issue is the spatial overlap and relative centers of the SNR and the background radiation field. In the scenario we propose here, the net radiation pressure within the SNR is important, and we assume that the radiation field of the cluster is not

dominated by sources that are spherically symmetric external to the SNR (so as to cancel the field in the SNR interior). The Jeans length in primordial gas is of order 1 pc, a distance that the radii of SN shells in our calculations exceed early in the SNR evolution (as shown below). Therefore, we assume approximate spherical symmetry and that the Population III cluster is not strongly off-center relative to the SNR.

The first SNe are required in this model to occur in halos whose virial temperature is at least 10^3–10^4 K, for two reasons. First, this is a criterion in the model of triggered star formation that we use here (Salvaterra et al. 2004). Second, the SN kinetic energies considered here (10^{51}–10^{53} ergs) do not exceed the binding energies of such galaxies, ensuring that we are dealing with subgalactic phenomena rather than dust transport to the IGM. A single 10^{53} erg SN can expel gas efficiently from low-mass minihalos of virial temperatures 100 K (corresponding masses of $\sim 10^6\ M_\odot$); even such small halos can, however, partly survive a 10^{51} erg SN (Bromm et al. 2003).

We assume that the dust from the first SNe is created on timescales of hundreds of days after the SN event (Todini & Ferrara 2001; Nozawa et al. 2003; Schneider et al. 2004) and solve for the density and temperature of the SNR as detailed below. In young remnants, the dust grains presumably form in cooling, metal-rich ejecta, which are slowly decelerated by interactions with gas in the SNR interior and by the reverse shocks. After the dust grains form through nucleation of ejecta material, they are subject to destruction through thermal sputtering by plasma (H and He ions) and by the passage of the reverse shock through the dense ejecta. We compute the sputtering within the SNR (Sedov-Taylor) interior, but do not compute the effects of reverse shocks. Some dust grains may survive these shocks, if a sufficient number reside in dense cold clumps. This may be indicated by observations of the Cas A SNR (Greidanus & Strom 1991; Hines et al. 2004), although whether the detected dust belongs to the SNR or to circumstellar material is controversial (Krause et al. 2004).

Those dust grains that survive are radiatively driven by the Population III radiation field and transported to varying distances as detailed below. We do not model the effects of the inhomogeneous density and radiation field arising from multiple stellar clusters or the nonuniform density and velocity structure within the SNR. We assume that the initial velocities of all the dust grains are of order 100 km s^{-1}, consistent with observations of the Cas A SNR (Fesen et al. 1987). We discuss the effects of varying the initial velocity of the dust grains in more detail in § 4.4.

For metal-free Type II SNe (Todini & Ferrara 2001), magnetites and ACGs (graphites) in general dominate the dust mass in the stellar progenitor range 12–35 $M_\odot$, with an increasing magnetite yield with rising SN explosion energies for 22–35 $M_\odot$. For the specific case of 22 $M_\odot$, the typical grain sizes are about 0.001 μm for magnetites, slightly lower values for silicates, and about 300 Å for graphites. In contrast, the dust mass from PISNe is strongly dominated by silicates, with a small, nearly constant yield of ACGs and a rapidly rising yield of magnetites with increasing stellar mass over 140–260 $M_\odot$. In addition, a 149 (250) $M_\odot$ parent star generates post-SN dust grains of characteristic sizes of 0.001 (0.01) μm, 0.01–0.1 (0.001–0.01) μm, and 0.01–0.1 (0.1) μm for magnetites, silicates and graphites, respectively. These trends of grain compound and size with stellar mass from Nozawa et al. (2003) and Schneider et al. (2004) use predictions of element nucleosynthesis from current hydrodynamical SN models. These results, combined with calculations of the chemical, temperature, and density evolution of the SN ejecta, determine which and when dust compounds can condense after the SN explosion and their subsequent growth. The temperature affects the order of grain formation, which in turn influences their characteristic sizes. In the PISN mass range, graphites condense first (at higher ejecta temperatures) and therefore tend to be larger in size relative to silicates and magnetites, which condense later. Thus, not all dust grains are created equal: there is a strong dependence of grain size and net yield on the star's mass, a point whose importance to the EMP stellar abundances is demonstrated below.

3.2. *Transport of Dust Grains*

The equation of motion of nonrotating spherical grains of mass $m_d = (4\pi/3)\rho_g a^3$ (with density ρ_g and radius a) under the effect of radiation pressure, gravity, and gas drag is given by

$$m_d \frac{dv}{dt} = F_r + F_g - F_{\rm drag}, \tag{1}$$

where the force F_r due to radiation pressure for a given source of luminosity L, acting on a grain at a distance r, is

$$F_r = \frac{L}{4\pi r^2 c}\pi a^2 \bar{Q}_{\rm pr}, \tag{2}$$

where $\bar{Q}_{\rm pr} = \bar{Q}_{\rm abs} + Q_{\rm sca}(1 - \langle\cos\theta\rangle)$. The averaging is done over the spectral energy distribution of the radiation field. We assume a primordial composition for the gas.

$Q_{\rm abs}$ and $Q_{\rm sca}$ are, respectively, the absorption and scattering coefficients, and $\langle\cos\theta\rangle$ characterizes the scattering property of the grain. The values of $Q_{\rm abs}$, $Q_{\rm sca}$, and $\langle\cos\theta\rangle$ for graphites and silicates are tabulated in Draine (1985). The values of $Q_{\rm sca}$ are typically much smaller than $Q_{\rm abs}$, and for our calculation we have used $Q_{\rm sca} = 0$, which makes the estimate of the radiation pressure on grains conservative. For the values of $Q_{\rm abs}$ for silicates we use the fit provided by Ferrara & Dettmar (1994), and for graphites we use the fits provided by Nath et al. (1999) for different ranges of incident photon energy. The radiation field is assumed to be Planckian with a radiation temperature T_*.

We have performed similar calculations for magnetites (Fe_3O_4). This compound could be produced in primordial SNe (Nozawa et al. 2003; Schneider et al. 2004), subject to the uncertainties in the explosion mechanism and mass cut of SNe associated with the first stars. For this work the role of magnetites is particularly important to consider, as the differential transport of graphite and silicate dust grains relative to those in iron compounds must be accomplished if we wish to explain the origin of the ultra–iron-poor EMP stars that have highly enhanced C, O, Mg, and Si relative to solar values. For magnetites, we have used the appropriate values of the absorption coefficients calculated from Mie scattering theory (S. Bianchi 2005, private communication).

The gravitational force on the grain is calculated, assuming a NFW profile (Navarro et al. 1997) and assuming the source of radiation to be at the cluster center, as

$$F_g = -\frac{GM_{\rm tot}(r)m_d}{r^2}, \tag{3}$$

where $M_{\rm tot}(r)$ is the total mass inside the radius r. Following Komatsu & Seljak (2001), one can define a characteristic radius $r_s = r_{\rm vir}/c$ for an object of total mass M collapsing at a redshift z and a concentration parameter c, where

$$r_{\rm vir}^3 = \frac{M}{(4\pi/3)\Delta_c(z)\Omega_m\rho_c(z)}, \tag{4}$$

where $\Delta_c(z)$ is the overdensity and $\rho_c(z) = 3H^2/8\pi G$ is the critical density of the universe. The overdensity $\Delta_c(z) \approx (18\pi^2 + 82x - 39x^2)/\Omega(z)$, with $x = \Omega(z) - 1$ and $\Omega(z)$ as the ratio of mean matter density to critical density at redshift z (Bullock et al. 2001). The density at this characteristic radius r_s is given by $\rho_s = \{c^3 M/[4\pi r_{\rm vir}^3 m(c)]\}$, where $m(c) = \ln(1 + c) - r/(1 + c)$. The total mass within a radius r can then be written as

$$M_{\rm tot}(r) = 4\pi\rho_s r_s^3 m(r/r_s). \quad (5)$$

To compute the drag force, we first calculate the charge on the grain, as detailed further in this section, and use equation (4) from Draine & Salpeter (1979a). We refer the reader to this paper for greater detail on this calculation. The drag force on the dust grain has two components: collisional drag, caused by the physical collision of grains with H and He atoms, and plasma drag, arising from the long-range Coulomb forces associated with the grain charge. Additional effects for the grain charge that arise from the grain's motion (Shull 1978) are relevant only when the grain's velocity exceeds the thermal velocity of protons and are not considered here.

Grains are charged by the photoelectric effect in the presence of the radiation field and collisions with electrons and protons. Coulomb drag is the dominant process in this calculation and strongly affects the motion and evolution of the grains. We do not include the effects of magnetic fields in primordial galaxies in this calculation, in the absence of a compelling theory as to such a field's structure and magnitude and the role of galactic amplification processes. The charging from the photoelectric effect depends on $Q_{\rm abs}$, the absorption coefficient of the grain (see above), and the radiation field J_ν. For a thermal gas with electron and proton densities n_e, n_p, and temperature T, the photoelectric current is given by

$$J_{\rm ph} = \int_{\nu_{\rm min}}^{\infty} Q_{\rm abs}(a, \nu) y_\nu \frac{4\pi J_\nu}{h\nu}\, d\nu, \quad (6)$$

where $\nu_{\rm min} = (w + eU)/h$ corresponds to the minimum energy for electrons to escape from the surface, w is the work function, and y_ν is the normalized photoyield. We use the fits for y_ν provided by Bakes & Tielens (1994).

Following Draine & Salpeter (1979b), we write the currents due to collisions with protons (with $x = eU/kT$, where $U = Z_{\rm gr}e/a$ is the grain potential, where $Z_{\rm gr}$ is the grain charge) as

$$J_p \approx n_p \left(\frac{kT}{2\pi m_p}\right)^{1/2} \quad (7)$$

and with electrons as

$$J_e = -n_e \left(\frac{kT}{2\pi m_e}\right)^{1/2}. \quad (8)$$

These currents are enhanced by Coulomb interactions by a factor of $g(x)$. For electrons $g_e(x) = \exp(x)$ for $x < 0$ and $g_e(x) = 1 + x$ for $x > 0$, and for protons $g_p(x) = \exp(-Z_{\rm gr}x)$ for $x > 0$ and $g_p(x) = 1 - Z_{\rm gr}x$ for $x < 0$ (Spitzer 1978). The charging timescales are much smaller than the transport timescale of the grains in our calculations, and therefore the grain charge can be calculated from the equilibrium condition at each radius: $J_{\rm ph} + J_p + J_e = 0$.

In addition to the equation of motion (eq. [1]), we also calculate the evolution in grain sizes due to sputtering. Grains are considered to be destroyed when they are reduced to 10^{-3} of their original size. For the case of magnetite grains, there are no published sputtering yields in the literature, and a detailed calculation of this quantity is beyond the scope of this work. Bianchi & Ferrara (2005) derived that graphite and olivine [$(Mg, Fe)_2 SiO_4$] grains have similar sputtering rates, as long as the grain velocities are at least 100 km s^{-1}, as we have assumed here. The theoretical expectation would be that the values for magnetite sputtering lie between those for silicates, which have similar binding energies per atom, and for metallic Fe (B. T. Draine 2005, private communication). The latter may be preferred if oxygen is preferentially sputtered from magnetite grains. For these reasons, we approximate the magnetite sputtering rate as that for pure Fe from Tielens et al. (1994); for consistency, we use the sputtering rates from these authors' calculations for graphites and silicates as well (see also eq. [3] of Seab & Shull 1983).

4. RESULTS

We present the main findings of our paper in this section in four parts in the following order: (1) the role played by a grain's area-to-mass ratio in determining its response to a radiation field; (2) a solution for the evolution of the densities and temperatures within primordial SNRs, which will provide the background conditions for grain transport; (3) using the results from (2) and earlier sections, a derivation the efficient transport of graphite and silicate grains relative to magnetites within SNRs, with the associated implications for the abundance ratios of Fe-poor EMP stars and the first-stars IMF; and (4) a quantification of the impact of varying a few of our model assumptions on the results in this work. At the end of each of the first three subsections, we present a brief summary of its findings in the broader context of the paper.

4.1. *Radiation Pressure on Dust Grains*

The dynamics of dust grains are determined by a complex interplay between gas density, temperature, and grain properties such as size, mass, density, and charging rate. The relevant considerations for this problem are (1) the ratio of the grain's effective area to mass, which is important for grain dynamics under radiation pressure and gravity, and (2) the relative values of the outward force due to radiation and gas drag, another important input to the grain's motion.

The effective area, also frequently referred to as the absorption cross section, is determined by the geometric area (πa^2) and the absorption coefficient $Q_{\rm abs}$. We plot the ratio of the effective area to the mass of the grains (in units of cm^2 g^{-1}) as functions of the wavelength of the incident radiation in Figure 2 for graphites, silicates, and magnetite grains. For each species, we show two cases, with grain radii $a = 0.001$ and 0.01 μm. We should note that for a Planckian radiation field with effective temperature $T_{\rm eff} = 5 \times 10^4$ K, the peak of the spectrum is at $\lambda \sim hc/2.82kT_{\rm eff} \sim 0.1$ μm. Such a hot radiation field is easily achieved in the atmospheres of metal-free stars of masses exceeding about 10 $M_\odot$ (Tumlinson et al. 2003; Bromm et al. 2001b). The curves show that smaller grains in general have larger ratios of area to mass, and graphites have the largest ratio, followed by silicates and then magnetites, a direct consequence of their respective grain densities of 2.2, 3.2, and 5.2 g cm^{-3}.

We therefore anticipate, in the context of SNRs resulting from Population III SNe in primordial galaxies, that graphite grains will be affected by radiation pressure more than silicate and magnetite grains, and small grains will experience greater radiation pressure than large grains.

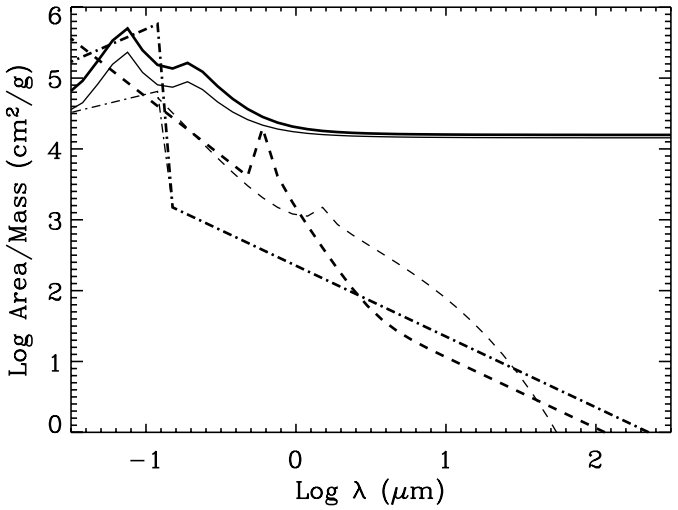

FIG. 2.—Ratio of effective area to grain mass plotted as a function of wavelength of the incident radiation, for graphites (*solid lines*), silicates (*dot-dashed lines*), and magnetite (*dashed lines*) grains. In each case, thick and thin curves denote grains of size $a = 0.001$ and 0.01 μm.

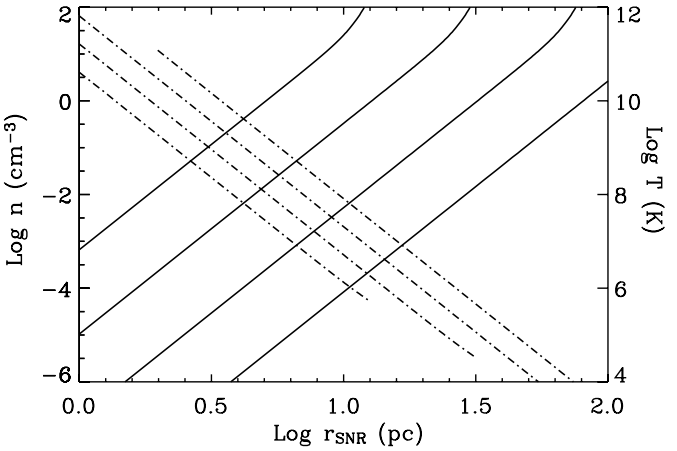

FIG. 3.—Evolution of the particle density (*solid lines*, *left y-axis*) and temperature (*dash-dotted lines*, *right y-axis*) in the SNR interior with radius in pc for an ambient density of 10 cm^{-3} and $E_{SN} = 10^{52}$ ergs and an assumed Sedov-Taylor self-similar solution. Within each set of lines, the curves from left to right are for $t = 10^4$, 10^5, 10^6, and 10^7 yr; these would move to the right for lower ambient densities (see text).

4.2. *SNR Evolution*

In order to calculate the transport of dust grains with the equations described in § 3, we need to assume approximate background gas temperatures and number densities within the SNR. Although we have not modeled the detailed density and velocity structure in this region, we assume parameter values that encapsulate the range of physical conditions expected within the SNR in the SN-induced star formation scenario. We show this in Figure 3, where the evolution of the density and temperature with interior radius in the SNR (not the SN shell radius) is plotted for times up to 10 Myr. We use Sedov-Taylor self-similar solutions and the analytic approximations of Kahn (1975) and Petruk (2000) for the temperature and density profiles in Figure 3, assuming a typical HN/PISN explosion energy $E_{SN} = 10^{52}$ ergs and an ambient gas density of 10 cm^{-3}. These parameters represent the typical conditions under which the fragmentation instability can occur in SN shells in primordial galaxies (Salvaterra et al. 2004), although densities of 10 cm^{-3} may only be achieved in the cold, star-forming cores of such galaxies.

The timescales on which SN shells form can be estimated from the equations describing the Sedov-Taylor phase of SNRs (Shull & Silk 1979). For the above parameters, the shell radius, velocity, and postshock temperature in the shell scale with E_{52} (SN energies of 10^{52} ergs), ambient density n_{10} (in units of 10 cm^{-3}), and time t_4 (in units of 10^4 yr) as

$$R_s = (12.7 \text{ pc}) E_{52}^{0.2} n_{10}^{-0.2} t_4^{0.4}, \quad (9)$$

$$V_s = (439 \text{ km s}^{-1}) E_{52}^{0.2} n_{10}^{-0.2} t_4^{-0.6}, \quad (10)$$

$$T_s = (2.58 \times 10^6 \text{ K}) E_{52}^{0.4} n_{10}^{-0.4} t_4^{-1.2}. \quad (11)$$

Applying the cooling criterion for the onset of radiative shell formation with free-free cooling from H^+ and He^{+2} ions leads to shell formation at times of

$$t_{\text{shell}} \sim (2.1 \times 10^4 \text{ yr}) E_{52}^{1/8} n_{10}^{-3/4}. \quad (12)$$

Thus, the SN shell has begun to form at about 10^4 yr, and the temperature has dropped sufficiently to lower sputtering rates within the shell. Figure 3 shows that, under these conditions and for the SN energies considered here, the typical size of SN shells is on the order of tens to at most hundreds of pc over timescales of 10 Myr. We also investigated cases with ambient densities of 1 cm^{-3}, where the lines in Figure 3 simply scale toward the right. At a given time and SN shell radius, the density within the SNR is almost 2 orders of magnitude lower in comparison to the 10 cm^{-3} case.

Figure 3 also reveals that at early times ($\lesssim 10^5$ yr) when the SN shell has advanced to about a few to 10 pc, typical densities and temperatures in the SNR interior are, respectively, on the order of 0.1 cm^{-3} and a few $\times 10^8$ K. Since the dust that survives post-SN processes such as the reverse shock is likely to be found in cooler gas, we conservatively assume ambient temperatures of 3×10^7 K (the value at about 6 pc at 10^4 yr) and an ambient density of 0.1 cm^{-3} within the SNR.

In summary, for a typical Population III SN with $E_{SN} = 10^{52}$ ergs, a SN shell begins to form in primordial galaxies at $\sim 10^4$ yr after the initial explosion and reaches distances of $\sim$10–100 pc in 10 Myr. The SNR interior remains hot on these timescales, and we assume background gas conditions of 3×10^7 K and 0.1 cm^{-3} in solving for dust grain transport within the SNR.

4.3. *Grain Dynamics*

We use the results of Schneider et al. (2004) and Todini & Ferrara (2001) for the formation of dust grains in SNe in primeval galaxies in order to assume the sizes of grains of different composition in our calculations. They found, as discussed earlier in this work, that for SNe with a progenitor mass of 149 $M_\odot$, the size distribution of magnetite grains peaked at $\sim$0.001 μm, and those of graphites and silicates at $\sim$0.04 μm. For stellar masses of 22 and 250 $M_\odot$, the characteristic grain sizes for magnetites/silicates/graphites are, respectively, of order 0.001/0.001/0.03 μm and 0.01/0.01/0.2 μm. These three masses span the range of SN progenitors considered here. We refer the reader to these papers and to Nozawa et al. (2003) for the detailed grain size distribution for various stellar masses.

We show in Figure 4 the position of dust grains under the combined forces of radiation, gas drag, gravity, and sputtering, using the above values for the initial sizes of grains of the relevant composition for the three representative stellar mass cases. We recall our model assumptions discussed earlier, that all grains are

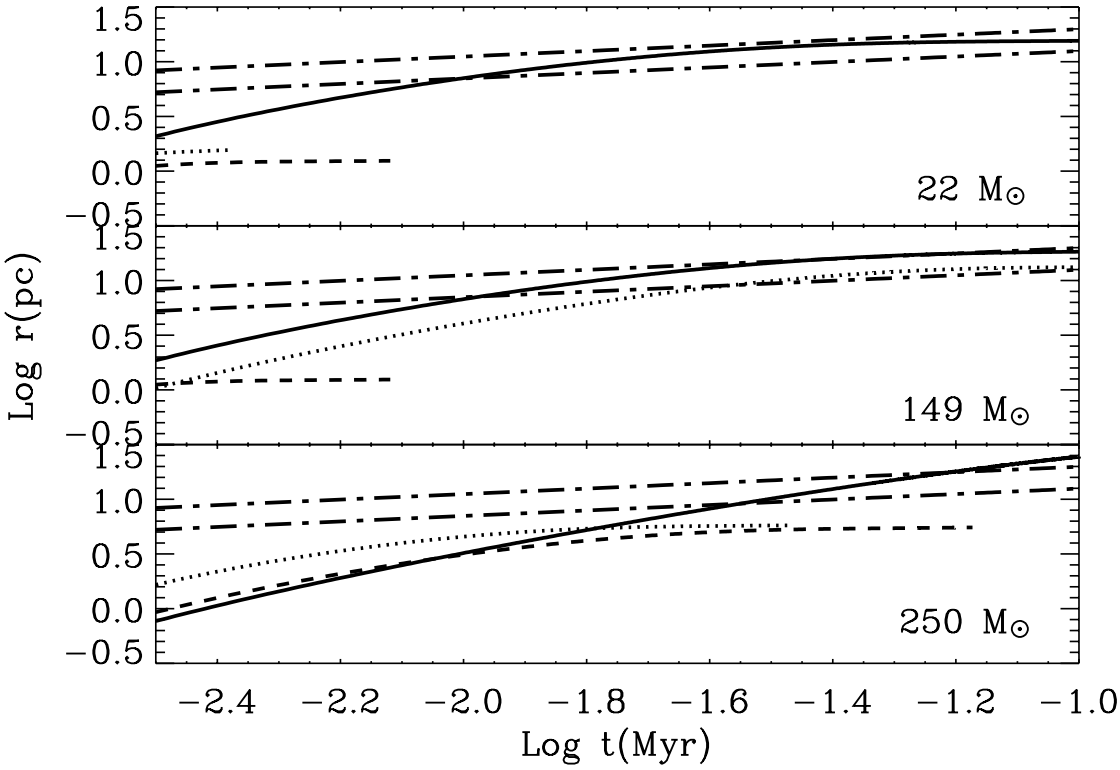

FIG. 4.—Positions of dust grains within SNRs in primordial galaxies, shown as a function of time as they are radiatively transported outward from the center of the SNR. Stellar masses of (*top*) 22, (*middle*) 149, and (*bottom*) 250 $M_\odot$ span the range of SN progenitors considered in this work. Solid, dotted, and dashed curves refer to graphites, silicates, and magnetite grains, respectively. The initial grain sizes for the compounds in each panel are detailed in the text. The two dash-dotted lines in each panel describe the adiabatic evolution of the SN shell radius for $E_{\rm SN} = 10^{52}$ ergs and ambient gas number densities of (*upper line*) 1 cm^{-3} and (*lower line*) 10 cm^{-3}. See text for discussion.

released at $r = 0$ with an initial speed of 100 km s^{-1}, that the luminosity of the central source is $L = 10^6\ L_\odot$ with a Planckian spectrum of effective temperature $T_{\rm eff} = 5 \times 10^4$ K, and that the temperature and gas density within the SNR are uniform at 3×10^7 K and 10^{-1} cm^{-3}, respectively. We do not use the temperatures and densities from the self-similar solutions shown in Figure 3 for two reasons. First, strong departures from a roughly constant product of density and temperature within the SNR occur only close to the SN shell. Second, the self-similar profile would indicate extremely high temperatures ($\gtrsim 10^{10}$ K) near the SNR center, which would destroy all dust grains promptly. Such a profile is an idealization in the most central regions, and it may not be a realistic representation of the physical conditions there.

Figure 4 shows the radiative transport of graphites, silicates, and magnetites, as well as two additional curves that represent the adiabatic evolution of the SN shell for an explosion energy of 10^{52} ergs and ambient densities of 1 cm^{-3} (*upper curves*) and 10 cm^{-3} (*lower curves*). Clearly, the SN shell advances to smaller distances for higher ambient densities, which could lead to more effective pileup of grains. The SN shell positions are computed using the Sedov-Taylor formalism in the appendices of Shull & Silk (1979) for the first 10^2 yr, and thereafter by solving the differential equations (2) and (3) in Salvaterra et al. (2004) without the radiative cooling term in equation (3). We note that the latter treatment accounts for the mass swept up by the shell, which is substantial by 10^4 yr and considerably slows the forward motion of the shell. Hence, the shell radii values in Figure 4 are significantly smaller than those from a simple Sedov-Taylor treatment for times exceeding 10^4 yr, e.g., 11 versus 19 pc at 10^4 yr for ambient densities of 1 cm^{-3}.

The curves in Figure 4 show that dust grains of sufficient size are driven by radiation equally effectively, irrespective of grain type, and that graphites, silicates, and magnetites may pile up in the SN shell well before 1 Myr. Although smaller grains experience radiation pressure more strongly (Fig. 2), they are destroyed on faster timescales because of greater relative loss of size. This is seen clearly in Figure 4, where graphites consistently reach the SN shell because of their relatively large size for all the displayed stellar masses, whereas the small magnetite grains are destroyed at the high SNR interior temperatures before arriving at the shell. As the temperature increases, the sputtering rates rise and compete with the decreasing Coulomb drag. Sputtering affects graphite and silicate grains as well, but given their typical grain sizes in the figure, significantly higher densities and/or temperatures ($\gtrsim 7 \times 10^7$ K) are required to boost sputtering and prevent shell pileup of these grains. This can also be achieved by having the SN explode into an ISM of lower ambient densities than we have assumed here, in which case the SN shell would advance to larger distances, leading to less effective pileup of dust grains. Transport through SNR interior temperatures that exceed $\sim$few $\times 10^7$ K will destroy grains of similar sizes at roughly the same radii and will not cause element segregation.

In the context of EMP stellar abundances, where silicate elements and carbon were often enhanced with respect to iron, the 149 $M_\odot$ case appears at first glance to offer the best explanation for reasonable parameter choices. The 22 $M_\odot$ case favors graphites alone, whereas a SN from a 250 $M_\odot$ star creates larger grains in general, leading to the eventual transport of graphites, silicates, and magnetites to the SN shell. The magnetite grains from 22 and 149 $M_\odot$ SNe are considerably smaller ($\sim$0.001 μm) and are sputtered away before they can arrive at the SN shell.

To fully reconcile these results with the current EMP data presented in § 2, there is an additional important factor to consider: the relative masses in these dust grains formed in primordial

SNe. The survival and deposition of any compound must be considered, along with its net yield. As discussed earlier, magnetites and graphites dominate the dust yield from 12–35 $M_\odot$ SNe, while PISNe from the stellar mass range 140–260 $M_\odot$ create mostly silicates, typically 1–2 orders of magnitude more by final mass than graphites or magnetites. When these trends are considered with those in Figure 4, we conclude that the mass range ~10–150 $M_\odot$ best explains the enhancement of carbon and silicate elements in Fe-poor EMP stars, with the lower end of this range being most appropriate for C-rich, Fe-poor EMP stars. High-mass PISNe, as seen in the 250 $M_\odot$ case, would predict a strong enhancement of silicates and iron relative to carbon, which is not matched by the data.

These results remain approximately true when compared with the predictions of dust grain sizes and mass yields from other works, such as Nozawa et al. (2003). These authors predict larger grain sizes and yields for silicates from a 25 $M_\odot$ star than we have assumed here for a 22 $M_\odot$ star from Todini & Ferrara (2001) and a mass output of graphites that depends strongly on the degree of mixing in the SN ejecta. The trends from Nozawa et al. (2003) would imply that more silicates from metal-free Type II SNe would reach the SN shell and that the transport of graphites from 10–260 $M_\odot$ stars would be more variable, depending on the physical conditions in individual SNe. These outcomes will only strengthen the connection to the EMP stellar data, where the elements Mg, Si, and O are typically overabundant relative to Fe at low [Fe/H], while this is true for C in only a fraction of the same EMP stars.

To summarize, current models indicate that primordial SNe create graphite and silicate grains of larger size and, for some stellar masses, in greater quantities than magnetites. This directly results in the more efficient transport of graphites and silicates through the SNR interior to the SN shells, where they could provide cooling that triggers second-generation star formation. A comparison with the abundance trends in Fe-poor EMP stars indicates a first-stars IMF in the mass range 10–150 $M_\odot$, *if* dust transport dominates the element ratios in these stars.

4.4. *Model Assumptions and Variations*

We now address a few remaining issues related to our model assumptions, starting with our estimate of the magnetite sputtering rate. The calculation of this quantity has two input parameters—the density and sputtering rate of a specific grain species. We recall that currently there exist no sputtering data for magnetites; the rate either for silicates (which has a similar binding energy per atom) or for pure metallic Fe can be used as an approximation. The magnetite grain density may be set to its measured value of 5.2 g cm^{-3} or to that of pure Fe (7.9 g cm^{-3}). There are therefore four possible combinations of these two parameters in calculating the sputtering of magnetite (recall that for magnetites in the above figures, we have assumed grain densities of 5.2 g cm^{-3} and a pure Fe sputtering rate).

We show in Figure 5 the time-dependent position of magnetite grains for these four parameter combinations for grain sizes of 0.001 μm. The curves that use silicate sputtering rates in general lie below and terminate earlier than those with pure Fe sputtering rates, as expected from the higher values of the first quantity. A perhaps less obvious result in Figure 5 is the larger distance to which the grains with higher density are transported. This reveals the complex nature of the problem of dust transport; as we emphasized earlier, individual trends of grain mass, size, and density do not combine predictably in a given problem. In this case, the difference between the trajectories of light (less dense) and heavy (more dense) particles is not simply extrapolated, as they are subjected to a position-dependent radiation field. One may have expected that heavier particles always have lower velocities than lighter particles. We calculated velocities for each of the cases in Figure 5 and find that the lighter particles do indeed move faster initially, but slow down more rapidly than do the grains with higher densities. We attribute this behavior to the effect of the decreasing values of the driving radiation field with distance. Another factor may be the increase of grain charge with decreasing grain density. This trend appears to hold for the physical conditions in the problem explored in this paper, where the charge increases from magnetites to silicates to graphites, leading to the greater slowing of lighter dust grains from gas drag. This is consistent with the results of Bianchi & Ferrara (2005) in the context of dust transport to the IGM. We emphasize that this anticorrelation between charge and grain density may be true only in the specific environment considered here and may not apply in other astrophysical situations. The main point that we wish to demonstrate through Figure 5 is that the curve corresponding to grain density 5.2 g cm^{-3} and a pure Fe sputtering rate lies intermediate to the other cases in the figure and justifies our earlier assumption of these values for magnetite grains.

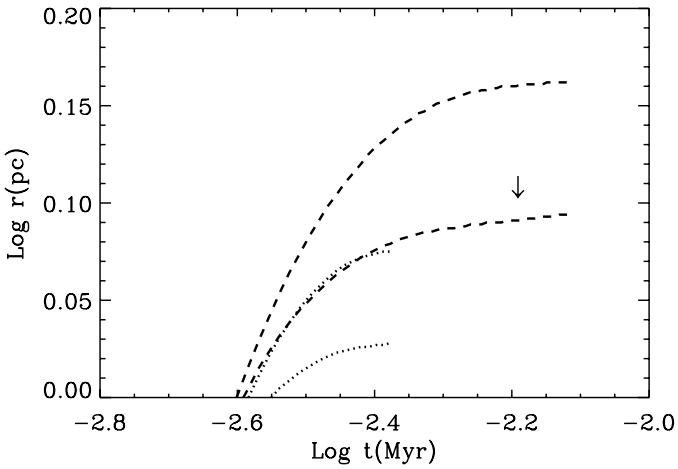

FIG. 5.—Radiative transport of magnetite grains, shown as a function of time with varying parameter values for grain density and sputtering rates. Dotted and dashed lines represent sputtering rates corresponding to those for silicates and pure Fe, respectively; within these cases, upper and lower curves correspond to densities of 7.9 and 5.2 g cm^{-3}, respectively (see text). The case assumed throughout the paper is marked with an arrow and is intermediate to the other cases. The initial size of all magnetite grains is assumed to be 0.001 μm.

Last, we have explored variations of the initial velocities of the dust grains. Lowering this quantity from our assumed value of 100–10 km s^{-1} does not change our results appreciably, because the speed to which the grains are accelerated by radiation pressure is itself of order 100 km s^{-1}. However, higher initial velocities of order 1000 km s^{-1} generally result in the grains being transported to greater radii. Depending on the role played by grain charge and gas drag, the grains may be driven out of the galaxy (see earlier references on dust transport to the IGM), and become less relevant for the problem of seeding metals for second-generation star formation in early halos.

5. CONCLUSIONS

We have investigated the radiative transport of dust within SNRs in primordial galaxies. We find that the differential transport of the primary dust compounds from the first SNe could be important for the problem of which metals seed the second generation of stars that form in the cooling shells of such SNe. The survivors of such second-generation star formation may be

detected as the EMP stars in the Galactic halo, whose metal abundance ratios provide clues to the chemical environment in which they formed. Calculations of the motion of dust grains within SNRs under the combined forces of the hot first-stars radiation field, gas drag, gravity, and sputtering reveal a complex interplay between grain size, charge, mass, density, and species. Our model requires that Population III star formation can continue for at least a few to 10 Myr in early halos, the lower limit on the sum of the lifetimes of massive stars and of the timescale for dust grains to cross the SN shells (typically well before 10^5 yr). In the context of this problem, our main findings are the following:

1. The role played by radiation pressure in the grain dynamics of different species is strongly influenced by the ratio of the grains' area to mass and decreases from graphites to silicates to magnetites. Within a given species, small grains are driven more effectively by radiation than are large grains.
2. We find that grain charge increases from magnetites to silicates to graphites, leading to greater Coulomb drag and loss of velocity for graphites and silicates relative to magnetites. However, a competing effect is the faster destruction of small grains, despite the stronger radiation pressure experienced by grains of decreasing size. The net result is that the generally larger graphite and silicate grains from the first SNe are more effectively driven and accumulate in the SN shells more than small magnetite grains.
3. If a dust transport scenario in primordial SNRs were to account for the segregation of elements observed in C- and silicate-rich, Fe-poor EMP stars in the Galactic halo, a metal-free stellar IMF spanning $\sim$10–150 $M_\odot$ offers the best explanation.
4. Higher temperatures and densities than those we have considered here will lead to increased sputtering and destruction of most grains and a loss of selective grain transport. At lower ambient ISM densities, the SN shell would advance further, reducing the possibility of grains of any species reaching the SN shell and mixing with star-forming gas.

A detailed prediction of the contribution of dust to the metallicity of second-generation stars is beyond the scope of this paper and is likely best studied through numerical simulations of primordial star-forming sites such as those cited earlier in this work. Clearly, dust transport can enrich such sites in elements that constitute the grains reaching the SN shell. A 200 $M_\odot$ star can produce up to 60 $M_\odot$ of dust (Schneider et al. 2004); if this is transported completely to the SN shell at a radius of 10 pc with an ambient density of 10 cm^{-3} and diluted into the swept-up mass of $\sim 10^3$ $M_\odot$, then supersolar metallicities of about 3 $Z_\odot$ in the shell can result. This is only an estimate of the average value. The real metallicity may be much higher or lower in cold star-forming clumps in the SN shell, depending on the efficiency of mixing processes and the role played by some of the transported elements in providing cooling pathways for primordial gas. Although it is beyond the scope of this work to fully compute how and when the transported dust grains get mixed into the SN shell gas, we may estimate it from the gravitational instability or free-fall timescale. This quantity is approximately $(G\rho)^{-1/2}$ and equals 10 Myr for hydrogen number densities of $\sim 10^2$ cm^{-3}. Therefore, if there is to be no significant delay from dust grain mixing prior to the onset of second-generation star formation, the gas in the SN shell has to exceed number densities of about a few $\times 10^3$ cm^{-3}.

There remain sizeable uncertainties in the modeling of dust transport in astrophysical environments, such as those detailed above, and factors related to the creation of dust in primordial SNe, such as the role of reverse shocks. Clearly, some dust does survive in these environments, as inferred from the recent detection of dust in a $z \sim 6.2$ QSO whose extinction curve indicates a SN origin (Maiolino et al. 2004). An additional point that we have not accounted for is the binarity fraction of the first stars, which can affect the mass loss from companion stars and reverse shock phenomena related to circumstellar material. Future spectroscopic analyses of Sloan-DSS and Hamburg/ESO survey data on EMP stars and observations of a variety of Galactic SNRs will help to address these important issues and ultimately constrain the formation sites and conditions of cosmological first- and second-generation star formation.

The authors thank Simone Bianchi and Bruce Draine for useful correspondence on the properties of magnetite and Yuri Shchekinov for helpful discussions. We thank an anonymous referee and S. Bianchi for useful comments on the manuscript. A. V. gratefully acknowledges the support of NSF grant AST 02-01670 through the NSF Astronomy and Astrophysics Postdoctoral Fellowship program. B. B. N. thanks the Fellows of JILA for their hospitality. J. M. S. acknowledges support at the Colorado astrophysical theory program from NASA LTSA grant NAG5-7262 and NSF grant AST 02-06042.

REFERENCES

Abel, T., Bryan, G. L., & Norman, M. L. 2000, ApJ, 540, 39
Aguirre, A. 1999, ApJ, 525, 583
Aguirre, A., Hernquist, L., Katz, N., Gardner, J., & Weinberg, D. 2001, ApJ, 556, L11
Aoki, W., Norris, J. E., Ryan, S. G., Beers, T. C., Christlieb, N., Tsangarides, S., & Ando, H. 2004, ApJ, 608, 971
Bakes, E. L. O., & Tielens, A. G. G. M. 1994, ApJ, 427, 822
Bianchi, S., & Ferrara, A. 2005, MNRAS, 358, 379
Briley, M. M., Cohen, J. G., & Stetson, P. B. 2004, AJ, 127, 1579
Bromm, V., Coppi, P. S., & Larson, R. B. 2002, ApJ, 564, 23
Bromm, V., Ferrara, A., Coppi, P. S., & Larson, R. B. 2001a, MNRAS, 328, 969
Bromm, V., Kudritzki, R. P., & Loeb, A. 2001b, ApJ, 552, 464
Bromm, V., & Loeb, A. 2003, Nature, 425, 812
Bromm, V., Yoshida, N., & Hernquist, L. 2003, ApJ, 596, L135
Bullock, J. S., Kolatt, T. S., Sigad, Y., Somerville, R. S., Kravtsov, A. V., Klypin, A. A., Primack, J. R., & Dekel, A. 2001, MNRAS, 321, 559
Cayrel, R., et al. 2004, A&A, 416, 1117
Christlieb, N., Gustafsson, B., Korn, A. J., Barklem, P. S., Beers, T. C., Bessell, M. S., Karlsson, T., & Mizuno-Wiedner, M. 2004, ApJ, 603, 708
Cohen, J. G., et al. 2004, ApJ, 612, 1107
Daigne, F., Olive, K. A., Vangioni-Flam, E., Silk, J., & Audouze, J. 2004, ApJ, 617, 693
Draine, B. T. 1985, ApJS, 57, 587
Draine, B. T., & Salpeter, E. E. 1979a, ApJ, 231, 77
———. 1979b, ApJ, 231, 438
Dwek, E., & Scalo, J. M. 1980, ApJ, 239, 193
Ferrara, A., & Dettmar, R.-J. 1994, ApJ, 427, 155
Ferrara, A., Ferrini, F., Barsella, B., & Franco, J. 1991, ApJ, 381, 137
Ferrara, A., Nath, B., Sethi, S. K., & Shchekinov, Y. 1999, MNRAS, 303, 301
Fesen, R. A., Becker, R. H., & Blair, W. P. 1987, ApJ, 313, 378
Frebel, A., et al. 2005, Nature, 434, 871
Greidanus, H., & Strom, R. G. 1991, A&A, 249, 521
Heger, A., & Woosley, S. E. 2002, ApJ, 567, 532
Hines, D. C., Rieke, G. H., Gordon, K. D., Rho, J., & Misselt, K. A. 2004, ApJS, 154, 290
Jones, A. P., Tielens, A. G. G. M., & Hollenbach, D. J. 1996, ApJ, 469, 740
Jones, A. P., Tielens, A. G. G. M., Hollenbach, D. J., & McKee, C. F. 1994, ApJ, 433, 797
Kahn, F. D. 1975, in Proc. 14th Int. Cosmic Ray Conf. (Munich), 3566
Komatsu, E., & Seljak, U. 2001, MNRAS, 327, 1353

Krause, O., Birkmann, S. M., Rieke, G. H., Lemke, D., Klaas, U., Hines, D. C., & Gordon, K. D. 2004, Nature, 432, 596
Loeb, A., & Haiman, Z. 1997, ApJ, 490, 571
Mackey, J., Bromm, V., & Hernquist, L. 2003, ApJ, 586, 1
Maiolino, R., Schneider, R., Oliva, E., Bianchi, S., Ferrara, A., Mannucci, F., Pedani, M., & Roca Sogorb, M. 2004, Nature, 431, 533
Nath, B. B., Sethi, S. K., & Shchekinov, Y. 1999, MNRAS, 303, 1
Navarro, J. F., Frenk, C. S., & White, S. D. M. 1997, ApJ, 490, 493
Nozawa, T., Kozasa, T., Umeda, H., Maeda, K., & Nomoto, K. 2003, ApJ, 598, 785
Pecker, J.-C. 1972, A&A, 18, 253
Petruk, O. 2000, A&A, 357, 686
Plez, B., & Cohen, J. G. 2005, A&A, 434, 1117
Qian, Y.-Z., & Wasserburg, G. J. 2005, ApJ, 623, 17
Salvaterra, R., Ferrara, A., & Schneider, R. 2004, NewA, 10, 113
Santoro, F., & Shull, J. M. 2006, ApJ, in press (astro-ph/0509101)
Schaerer, D. 2002, A&A, 382, 28
Schneider, R., Ferrara, A., Natarajan, P., & Omukai, K. 2002, ApJ, 571, 30
Schneider, R., Ferrara, A., & Salvaterra, R. 2004, MNRAS, 351, 1379
Seab, C. G., & Shull, J. M. 1983, ApJ, 275, 652
Shull, J. M. 1978, ApJ, 226, 858
Shull, J. M., & Silk, J. 1979, ApJ, 234, 427
Shustov, B. M., & Vibe, D. Z. 1995, Astron. Rep., 39, 578
Spitzer, L. 1978, Physical Processes in the Interstellar Medium (New York: Wiley)
Tielens, A. G. G. M., McKee, C. F., Seab, C. G., & Hollenbach, D. J. 1994, ApJ, 431, 321
Todini, P., & Ferrara, A. 2001, MNRAS, 325, 726
Tumlinson, J., & Shull, J. M. 2000, ApJ, 528, L65
Tumlinson, J., Shull, J. M., & Venkatesan, A. 2003, ApJ, 584, 608
Tumlinson, J., Venkatesan, A., & Shull, J. M. 2004, ApJ, 612, 602
Umeda, H., & Nomoto, K. 2003, Nature, 422, 871
Venkatesan, A., & Truran, J. W. 2003, ApJ, 594, L1
Wada, K., & Venkatesan, A. 2003, ApJ, 591, 38